Solar Energy Materials & Solar Cells 93 (2009) 1103–1109

Contents lists available at ScienceDirect

Solar Energy Materials & Solar Cells

journal homepage: www.elsevier.com/locate/solmat

Optimization of lead- and cadmium-free front contact silver paste formulation to achieve high fill factors for industrial screen-printed Si solar cells

Seong Je Jeon [a,b], Sang Man Koo [a], Seon Am Hwang [b,*]

[a] Hybrid Nono Particle Laboratory, Department of Chemical Engineering, Hanyang University, Seoul 133-791, South Korea
[b] Taiyo Ink MFG. Co., Ltd., Research Institute, Electronic Material Division, 1058-8, Shingil-dong, Ansan-City, Gyeonggi-do 425-839, South Korea

ARTICLE INFO

Article history:
Received 9 November 2007
Received in revised form
27 December 2008
Accepted 8 January 2009
Available online 9 March 2009

Keywords:
Lead-free front contact
Silver paste formulation
Screen printed
Silicon solar cell

ABSTRACT

Screen-printed n^+–p–p^+ solar cells were fabricated on Cz single crystalline Si material, with a 45 Ω/sq emitter and PECVD SiNx antireflective coating with a thickness of 700 Å, using different Ag pastes and commercial leaded reference paste (CN33-462, Ferro Corp.). Ag and Al contacts were co-fired using a mass-production line equipped with mesh belt conveyer furnace systems (Centrotherm thermal solution GmbH & Co. KG). The average results for single crystalline Si solar cells (156 cm^2) are: $I_{sc} = 5.043$ A, $V_{oc} = 0.621$ V, $R_s = 0.0087$ Ω, $R_{sh} = 15.3$ Ω, FF = 0.773, and $E_{ff} = 16.45\%$. R_{sh} and fill factor values of fabricated cells were slightly higher when compared with the commercial leaded Ag paste, although cells were fabricated by metallizing the lead-free silver pastes. For the lead-free Ag paste used in this study, the line pattern continuity is retained with improved edge definition in sharp contrast to that of reference Ag paste. Average value of R_s was also equivalent approximately to that of the leaded Ag paste.

1. Introduction

As is well known, relatively grave concern was paid to the applications of lead/cadmium-free silver or aluminum pastes in a photovoltaic market due to restriction of the use of certain hazardous substances (RoHS) directive from European Union for electric and electronic materials and their devices [1].

To date, there have been various researches regarding metallization of lead/cadmium-free pastes which have been already commercialized for production of silicon solar cells. Bahr et al. [2] reported lead/cadmium-free metallization for industrial solar cells and modules. Hoornstra et al. [3] also demonstrated that lead-free frit formulation resulted in solar cells with same efficiency and fill factor (FF) as for the leaded reference paste. Nevertheless, there remains an unexplained aspect of the know-how of paste formulations and its manufacturing technique. Moreover, when the lead-free glass frit was used, the reason for the increase of series resistance (R_s) still remains obscure.

The purpose of the present paper is to offer performance evaluations and characteristics of solar cells fabricated using the lead/cadmium-free front side Ag pastes optimized via design of compositions in a mass-production environment.

2. Experimental

2.1. Materials

Silver powder (KDSP-3000, Kornatech Co., Ltd., 99.9%), glass frits (KSGP01∼04, Kornatech Co., Ltd., 99%), which consisted of Bi_2O_3–B_2O_3–Al_2O_3–ZnO–Na_2O composite system and others, bismuth (III) oxide (Bi_2O_3, Aldrich, 10 μm, 99.9%), calcium oxide (CaO, anhydrous, Aldrich, 99.99%), magnesium oxide (MgO, Aldrich, 99.99%), aluminum oxide (Al_2O_3, Sigma-Aldrich, 5 μm, 99.7%), tantalum(V) oxide (Ta_2O_5, Aldrich, <5 μm, 99.99%), ethyl-cellulose (ETHOCEL STD, Dow chemical), α-terpineol ($C_{10}H_{18}O$, Acros, 99%) and 2-ethoxyethyl acetate ($C_6H_{12}O_3$, Samchun chemical, 99%) were used as received.

2.2. Cell fabrication

Eight types of the screen-printed n^+–p–p^+ solar cells were fabricated on $5'' \times 5'' \times 200\,\mu m^3$ Cz single crystalline Si wafer using different lead-free Ag pastes. In order to compare the electrical performance of fabricated cells, an additional reference cell was also fabricated with commercial leaded silver paste (CN33-462) available from Ferro Corporation.

These cells were fabricated as follows: for the removal of impurities and defects, wafers were treated first with a solution of

* Corresponding author. Tel.:+82 31 491 9250; fax: +82 2 492 2710.
E-mail address: rusun@taiyoink.co.kr (S.A. Hwang).

0927-0248/$ - see front matter © 2009 Published by Elsevier B.V.
doi:10.1016/j.solmat.2009.01.003

sodium hydroxide and washed in water purified by distillation and deionization. Conventional phosphorus diffusion was performed at 875 °C using a liquid $POCl_3$ source to obtain the n^+ emitter, leading to an emitter with a sheet resistance of around 45 Ω/sq. The next step, according to Lauinger's method [4], plasma enhanced chemical vapor deposition (PECVD) SiN_x single layer antireflective coating with a reflective index of 2.01 and a thickness of 700 Å was approximately deposited on the front side. These cells were then isolated using an automatic dicing saw. Subsequently, 48coating microstripelines of width 120 μm were screen printed on top of the SiN_x antireflective layer using mesh screen (count of 325) and dried at 200 °C. Two groups of Ag paste each having the different glass frits and inorganic additives were processed. In Table 1, we have summarized the details of the glass frits and inorganic additives in paste formulations.

In cases of the pastes (FS01∼04) without inorganic additives, their compositions have only varying size and content of glass frits with constant ethyl-cellulose to silver weight ratio of 1/49 and appropriate amount of solvents. All the solvents used in these pastes were composed of α-terpineol and 2-ethoxyethyl acetate with ratio set to 2/1 by weight for ease of screen printing. On the other hand, for FS05∼08 pastes, Bi_2O_3, Al_2O_3, MnO_2, MgO, CaO and Ta_2O_5 were additionally formulated where they can act as an inorganic binder or functional material. All the pastes used in this study were uniformly mixed by three roll milling.

For all experiments the same aluminum rear paste (TSP-5000, RP01) to form an alloyed Al back surface field (Al–BSF) and silver/aluminum pastes (TSP-5000, BE01), designed to use for bus bar and grid application from Taiyoink MFG. Co. Ltd., were sequentially screen printed on the backside and dried at 200 °C, and then co-fired at a set point of 910 °C (peak firing temperature) and belt speed of 3300 mm/min for Ag front metallization and Al-BSF alloy in the mesh belt conveyer furnace. The amount of Al pastes printed on the wafer was 0.045 g/sq. inch.

2.3. Characterization

The resulting cells were also characterized by the Belval S.A. Company model Pasan CT801 cell tester under standard test condition (156 cm^2; AM1.5; 25 °C; 1.0 kW/m^2) and their cross-section images were observed by field-emission scanning electron microscopy (FE-SEM, JEM-6340F, JEOL). The morphology and size of glass frits were also observed by FE-SEM. The transparency of the screen-printed, dried and fired glass pastes films was analyzed by a UV/Vis spectrophotometer (Optizen 2120 UV, Mecasys Co., Ltd.) on a soda lime silicate glass. After the front contact firing, an absolute line shrinkage and edged definition were observed by means of video microscope equipment (Xi-CAM, Besteckvision Co., Ltd.) with a commercial leaded reference paste. In addition, CAMECA IMS-6F magnetic sector secondary ion mass spectrometry (SIMS) is used in this research for the P concentration and depth profiling in the emitter region forms front contact silver grids. Cs^+ was used as a source of the primary ions. A beam of Cs^+ liquid metal ions, generated by thermal evaporation and ionization, was purified by mass filter. The impact energy of the primary ion beam was 15 keV. The primary current was approximately 100 nA. The primary ion beam was raster scanned over an area of $200 \times 200\ \mu m^2$ and its diameter was approximately 30 μm (Φ). The glass and silver layers were etched off for this measurement.

Table 1
Detail of the glass frits and inorganic additives in paste formulations.

Paste ID	Glass frit	wt%	Inorganic additives (wt%)					
			Bi_2O_3	Al_2O_3	MnO_2	MgO	CaO	Ta_2O_5
FS01	KSGP01	3.05	–	–	–	–	–	–
FS02	KSGP02	3.32	–	–	–	–	–	–
FS03	KSGP03	3.92	–	–	–	–	–	–
FS04	KSGP04	4.38	–	–	–	–	–	–
FS05	KSGP01	3.05	1.0	0.2				0.2
FS06		3.05	1.0		0.2			0.2
FS07		3.05	1.0			0.2		0.2
FS08		3.05	1.0				0.2	0.2

3. Results and discussion

The emitter doping profiles have an effect on the solar cell performance. As reported in Ref. [5], the specific contact resistance (ρ_c) and emitter sheet resistance (R_e) are inversely proportional to the surface dopant concentration (N_D), while for a well-passivated surface, emitter saturation current density (J_{oe}) and the photocurrent loss are directly proportional to N_D. Junction depth also greatly influences the junction shunting, photocurrent loss and J_{oe}. Therefore, in order to evaluate the cell performance, emitter doping profiles were preferentially examined by SIMS measurements. The phosphorus diffusion resulted in a 45 Ω/sq emitter with a peak concentration of 2.72E20P/cc and junction depth of ∼0.32 μm. Under this emitter characteristic, the lead-free front contact silver pastes having the optimized value of R_s and R_{sh} at conventional firing temperature were formulated. The cells with 45 Ω/sq emitter were fabricated using commercial leaded reference paste and different lead-free front contact silver pastes, which were manufactured with various lead-free glass frits and inorganic additives. The results of optimum values of electrical performance, FF_s and conversion efficiencies for the cells fabricated are summarized in Table 2.

KSGP series glass frits used are comprised of the same composition $78.5Bi_2O_3$–$12ZnO$–$7.4Al_2O_3$–$1.5B_2O_3$–$0.6Na_2O$ (wt%) containing 2.3 mol% of Ag_2O and others. Thermal coefficient of expansion (TCE) is approximately $\sim 90 \times 10^{-7}\ °C^{-1}$, which is similar to that of the Si wafer. Other thermal properties such as glass transition temperature (T_g) and softening temperature (T_s) were designed to be between 400–410 and 420–430 °C, respectively. As far as we know, KSGP series glass frits in the thermal properties have no size effects. In this study, the effects of the content and size of glass frits on the front metallization and electrical performance of the resulting cell were investigated. Fig. 1 shows the SEM micrographs of glass frits with a different mean particle size (D_{50}), 1.2–4.0 μm.

Transmittances of the four different glass pastes have been evaluated for the purpose of obtaining a metallization quality comparison. Fig. 2 shows the UV–VIS spectra of glass paste thick films screen-printed and fired on soda lime silicate glass in the wavelength range 300–800 nm. The glass pastes were formulated with the composition of the glass powder and organic vehicle, which consisted of α-terpineol, ethyl-cellulose and 2-ethoxyethyl acetate, under the same constituents and contents. As can be seen in Fig. 2, the transmittance of the KSGP01 glass paste thick film is the highest, and it significantly decreased with increase in their mean particle size. From these results it might be deduced that the difference of the transmittance is due to the predominant voids, which were formed by burning of ethyl-cellulose resin and secondary influences caused by pores inside the glass frits themselves after being fired. The increase of the void size in the fired glass matrix is also caused by glass frits with a large mean particle size. For these reasons, the KDGP04 glass paste containing glass frits with a large mean particle size eventually scatters the

Table 2
Electrical performances of the cells fabricated with different lead-free front contact silver paste and commercial-leaded reference paste.

Cell ID (paste[a])	V_{oc} (mV)	I_{sc} (A)	V_{mp} (mV)	I_{mp} (A)	P_{max} (W)	R_s (Ω)	R_{sh} (Ω)	FF_s (%)	$E_{ff.}$ (%)
C1 (FS01)	629	5.003	515	4.594	2.364	0.0093	18.5	76.4	16.08
C2 (FS02)	615	5.052	507	4.558	2.312	0.0097	5.3	74.4	15.70
C3 (FS03)	609	4.976	497	4.441	2.208	0.0110	6.1	72.9	15.02
C4 (FS04)	611	4.977	484	4.514	2.184	0.0130	8.4	71.9	14.86
C5 (FS05)	618	4.975	516	4.579	2.361	0.0090	16.1	76.7	16.06
C6 (FS06)	619	5.017	516	4.586	2.367	0.0099	14.8	76.2	16.10
C7 (FS07)	623	5.014	518	4.628	2.398	0.0089	9.8	76.8	16.31
C8 (FS08)	621	5.043	521	4.637	2.418	0.0087	15.3	77.3	16.45
C9 (commercial paste[b])	609	4.948	511	4.423	2.259	0.0083	4.3	74.9	15.37

The cells (C1–C8) correspond to paste types FS01–FS08, respectively.
[a] Paste compositions indicated in Table 1.
[b] CN33-462 available from Ferro corporation.

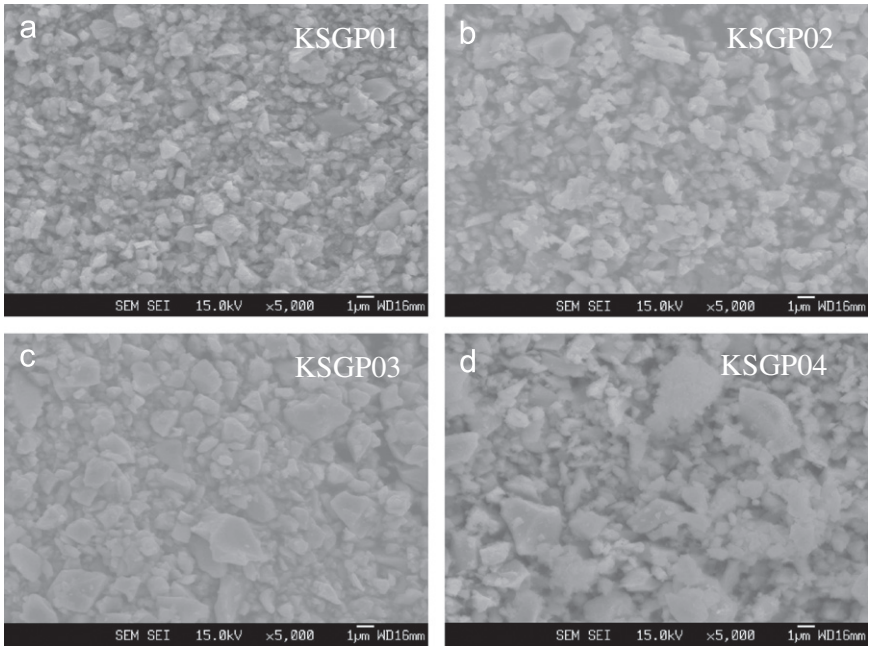

Fig. 1. SEM micrographs of glass frit powders with the different mean particle sizes: (a) KSGP01 ($D_{50} = 1.2\,\mu m$), (b) KSGP02 ($D_{50} = 2.1\,\mu m$), (c) KSGP03 ($D_{50} = 2.8\,\mu m$) and (d) KSGP ($D_{50} = 4.05\,\mu m$).

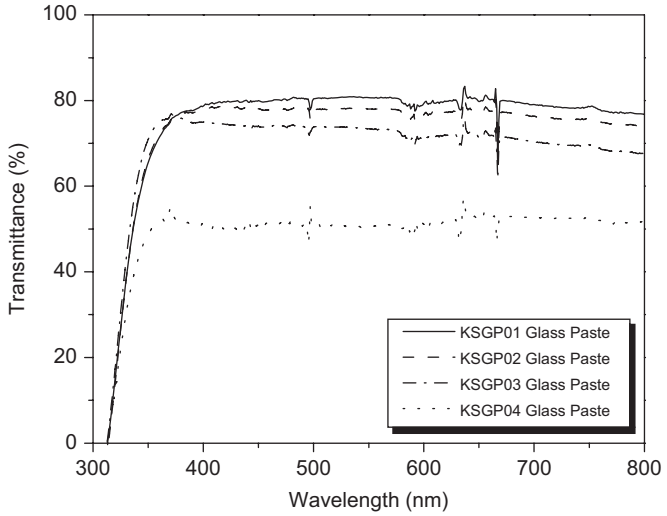

Fig. 2. Transmittance patterns of the different glass pastes after being fired at 600 °C for 30 min.

incidence and lowers transmittance. As will be discussed later, the difference of these results was also clearly confirmed by the observation of SEM cross-section images for the front contact silver pastes. The pastes containing glass frits with a large mean particle size do not allow for continuous contact formation in Si–Ag alloys due to the poor contact and metallization quality. From all this it should be clear that control technique, a glass frit, can have an influence on the silver front contact metallization quality during the firing step and what ultimately determines the contact quality is how well glass frits are controlled in precise amounts and its size.

Fig. 3 shows the relationship between the FF and amounts of glass frit in pastes through the series experiments using various lead-free glass frits. In all cases, the value of FF_s increases with increasing amounts of glass frits in pastes, reaching the maximum, and then decreases. The highest FF value of 76.4% was obtained when the KSGP01 ($D_{50} = 1.2\,\mu m$) glass frit was used. Unfortunately, although an amount of the glass frit used has been optimized, the cells fabricated using the glass frits with a large mean particle size had a lower FF and conversion efficiency (cell C2–C4, see Table 2). Consequently, the high FF_s and conversion

efficiencies could be obtained by using less glass frit when the glass frit with a small mean particle size was used.

The shrinkage of reference pastes in the finger line patterns increases considerably with increasing firing temperature, as observed in the optical microscope images in Fig. 4(a) and (b), while the line pattern continuity for lead-free FS01 silver pastes is remarkably retained with improved edge definition in sharp contrast to that of reference Ag paste at high firing temperatures (see Fig. 4(c) and (d)), indicating that the line and space resolution or their edged definition of finger line widths is improved controlling glass frits.

The corresponding *I–V* characteristic is described by the Shckley solar cell equation [7]

$$I = I_{ph} - I_0(e^{qV/k_BT} - 1) \quad (1)$$

where k_B is the Boltzmann constant, T is the absolute temperature, $q(>0)$ is the electron charge, and V is the voltage at the terminals of the cell. I_0 is the diode saturation current and I_{ph} is the photogenerated current that is closely related to the photo flux incident on the cell and its dependence on the wavelength of light is frequently discussed in terms of the quantum efficiency or spectral response. [7]

As is well known, the *I–V* characteristic of a solar cell in practice usually differs to some extent from the ideal characteristic (1). The solar cell may contain series (R_s) and shunt (R_{sh}) resistances, leading to a characteristic of the form. Thereby, the effect of the second diode and of R_s and R_{sh} on the *I–V* characteristic of the solar cell is given by

$$I = I_{ph} - I_0\{\exp[(V + IR_s)/k_BT - 1]\} - I_{02}\{\exp[(V + IR_s)/2k_BT - 1]\} - (V + IR_s/R_{sh}) \quad (2)$$

In addition, the effect of R_s on FF can also be allowed:

$$FF = FF_0(1 - r_s) \quad (3)$$

where r_s is expressed by R_sI_{sc}/V_{oc} and FF_0 is the FF of the cell without the influence of R_s and R_{sh}. That is also determined, to an excellent accuracy, by the approximate expression [7]

$$FF_0 = [V_{oc} - \ln(V_{oc} + 0.72)]/(V_{oc} + 1) \quad (4)$$

and using inclusive expression for overall conversion efficiency η [8]:

$$\eta = I_{mp}V_{mp}/P_{light} = FFI_{sc}V_{oc}/P_{light} \quad (5)$$

In Eq. (5), P_{light} stands for the incident power on the cell, and V_{mp} and I_{mp} are, by definition, the voltage and the current at the optimal operating point. Ultimately, electrical parameters such as I_{sc} (short circuit current), V_{oc} (open circuit voltage) and FF determine the conversion efficiency of the solar cell. Eqs. (2–5) predicate the contribution to efficiency decreases or power losses comes from the influences of R_s and R_{sh} in solar cells. Hence, it is most important that formulated pastes having the two optimized factors, i.e., the minimum R_s and maximum R_{sh}, are required for the solar cell to function at its best because they are directly important factors that affect $I(V)$ and FF values. Also, considering another aspect of the relation between voltages and resistances, in the region below 0.15 V current is mainly determined by R_{sh}, while in the region around 0.6 V, R_s has a considerable influence on the cell performance [8]. For this reason, we can expect that R_s mainly affects cell performance in our study. Here, the values of R_{sh} and R_s are plotted in Fig. 5 as functions of the amount of KSGP01 glass frit (wt%) in FS01 pastes. Fig. 5 explains why proper quantity of glass frits in pastes gives superior FF_s or higher $V_{oc}(I_{sc})$ values compared to excess or deficient quantities. Accordingly, a control technology of the glass frit size and the amount in pastes can evidently improve R_s and R_{sh}, allowing higher FF_s and conversion

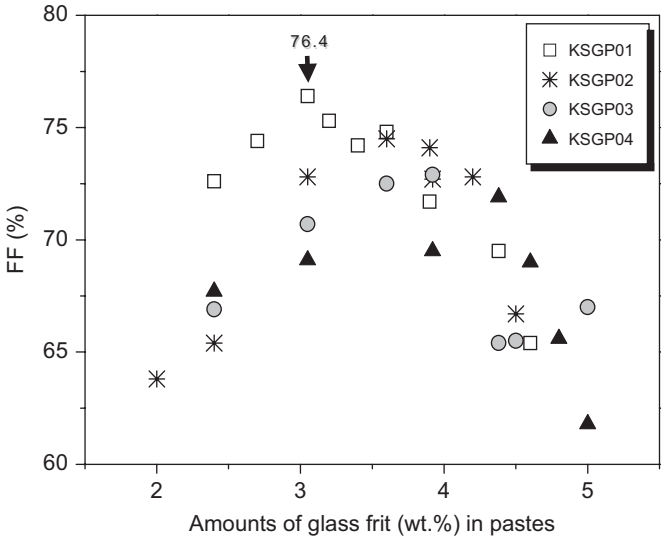

Fig. 3. Influence of glass frits with a different mean particle size as a function of their contents in pastes on the FF of solar cells.

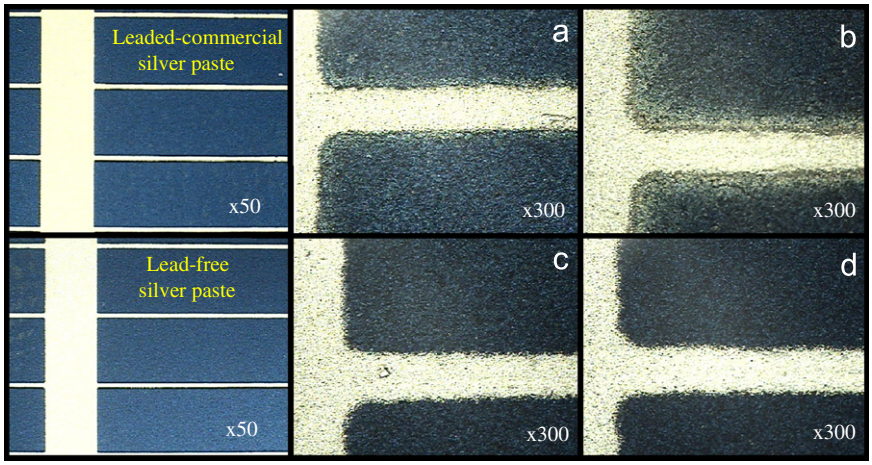

Fig. 4. Optical microscope images of fired silver front pastes corresponding to (a) Ferro CN-33-462 (peak fired temperature, T_{peak}: 750 °C), (b) Ferro CN-33-462 (T_{peak}: 910 °C), (c) FS01 (T_{peak}: 750 °C) and (d) FS01 (T_{peak}: 910 °C) pastes.

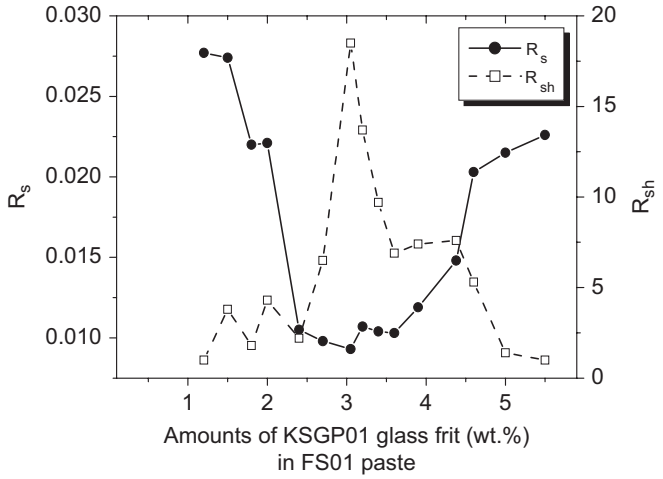

Fig. 5. The change of the series resistance (R_s) and shunt resistance (R_{sh}) as a function of amounts of KSGP01 glass frit (wt%) in FS01 pastes.

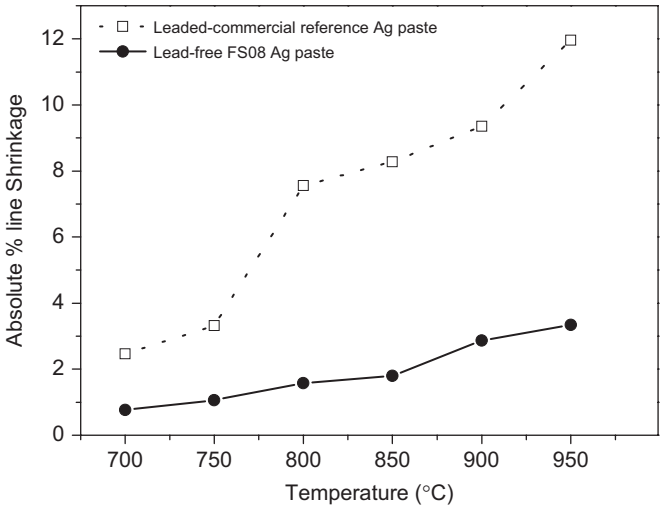

Fig. 6. The dependence of shrinkage in fired line patterns as a function of firing temperature.

efficiencies. All that considered, therefore, no less significant is the fact that the KSGP01 glass frit with small mean particle size has an advantage with regard to low R_s and higher FF_s and conversion efficiencies can be achieved by decreasing R_s values through controlling quantity of glass frits as well as mean particle size, and glass frit control technique is helpful for the good cell performance.

On the other hand, it is our intention to address the paste formulation of another type (see FS05∼08 pastes formulation in Table 1) to achieve better cell performance under the optimum condition of the glass frit content (3.05 wt% in pastes) and its size ($D_{50} =$ 1.2 μm). Inorganic additives for higher cell performances mainly consist of various constituents from four standpoints: (i) Bi_2O_3 and MnO_2, which provide more favorable binding and adhesion properties as a fluxing agent and better electrical conductivity, respectively; (ii) CaO and Al_2O_3, which enable decrease in the stress caused by a difference of thermal coefficient of expansion during firing; (iii) Ta_2O_5, which promotes a function of antireflection and transmission due to the high refractive index (∼2.26) and transmittance at blue violet region; lastly, (iv) magnesium (3.65 eV) and calcium (2.9 eV) sources with a low work function originated from MgO and CaO perform the function as a material with low junction barriers (<0.5 eV) between metal and n-type Si. And by this way, as expected, it was also observed that the C5–C8 cells that used the smallest glass frit, inorganic binder and additives had conversion efficiencies of above 16%, which was slightly higher than that of C2–C4 cells (14.86–15.7%) that only used larger size of glass frits. Additionally, replacing 0.2wt% of Al_2O_3 or MnO_2 with the same amount of MgO or CaO leads to an increase in conversion efficiency from 16.06–16.1% to 16.31–16.45%. Both C5 and C6 cells are comparable to the C1 cell. However, C7 and C8 cells are superior to the C1–C4 cells. Significantly, the highest values of FF (∼77.3%) and conversion efficiency (∼16.45%) are to be found for the cell fabricated with FS08 paste containing the smallest glass frit and inorganic additives such as Bi_2O_3 and CaO. In addition, the dependence of shrinkage in fired line patterns is also shown in Fig. 6 as a function of the firing temperature. As expected, the absolute percentage line shrinkage for the reference paste rapidly increases from ∼2% to above 10%. In contrast, that of lead-free FS08 pastes slightly increases from about 1% to 3%, when the firing temperature increases from 700 to 950 °C. These results are similar to those of Rane et al. [6] who also observed that the Ag thick films with Bi_2O_3 as a binder show a uniform and dense granular structure and grain growth at high firing temperature.

As in C2, C3 and C4 cells, increasing the mean particle size of glass frits above 2 μm resulted in lower R_{sh} values due to increase of Ag concentration at near junction regions after firing, and this in turn causes the increase of junction leakage current and lower V_{oc}. To be exact, the Ag paste formulated using glass frits of large mean particle size tend to have a higher junction shunting and leakage rate because of impurity incorporation, from the Ag paste containing glass frits into the junction region, caused by strong and partial Si etching of these glass frits. The shape of the irregular and discontinuous metallization is also attributed to excessive Si etching by the frit. As already discussed, however, these problems ultimately can be overcome through the addition of inorganic binders and using the smallest glass frits as seen in Fig. 7(e) and (f). In all cases, though the formation of the void in the silver matrix is attributed to burning of ethyl-cellulose resin after being fired, what stands out most from this study is the continuous formation of Ag–Si alloys between the interface regions for the cells fabricated using FS05 and FS08 paste. Moreover, silver matrix containing Bi_2O_3 as an inorganic binder shows relatively less voids after being fired. These results can be clearly observed in the cross-sectional SEM images of C5 and C8 cells.

On the other hand, for the C1 cell, the high R_{sh} and FF values may be attributed to the use of the glass frit with a small mean particle size and shallow silver penetration depth into Si from Ag–Si interface regions under the condition of the adequate junction depth and surface dopant concentration. These results agree with the reports by Sridharan et al. [9] and Khadilkar et al. [10] Thus, it could be concluded that the optimum formulation for better conductivity, higher density of the silver matrix compact and continuous contact formation of lead-free silver pastes could be designed by the addition of inorganic additives with the smallest glass frit (KSGP01) of 3.05 wt% in pastes.

From the comparison of the Ag–Si interface contact structures shown in Fig. 7, we can explain that added Bi_2O_3 might act as a fluxing agent, as was attempted for the development of Ag thick films using oxide binders [6]. These SEM examinations obviously reveal continuously better contact formations for the pastes containing Bi_2O_3 in comparison to any other paste without inorganic additives. Therefore, one assumption we can draw from this remarkable result is that the reaction $3Si+2Bi_2O_3 \rightarrow 3SiO_2+4Bi$ contributes to the etching of Si and SiN_x antireflective coating

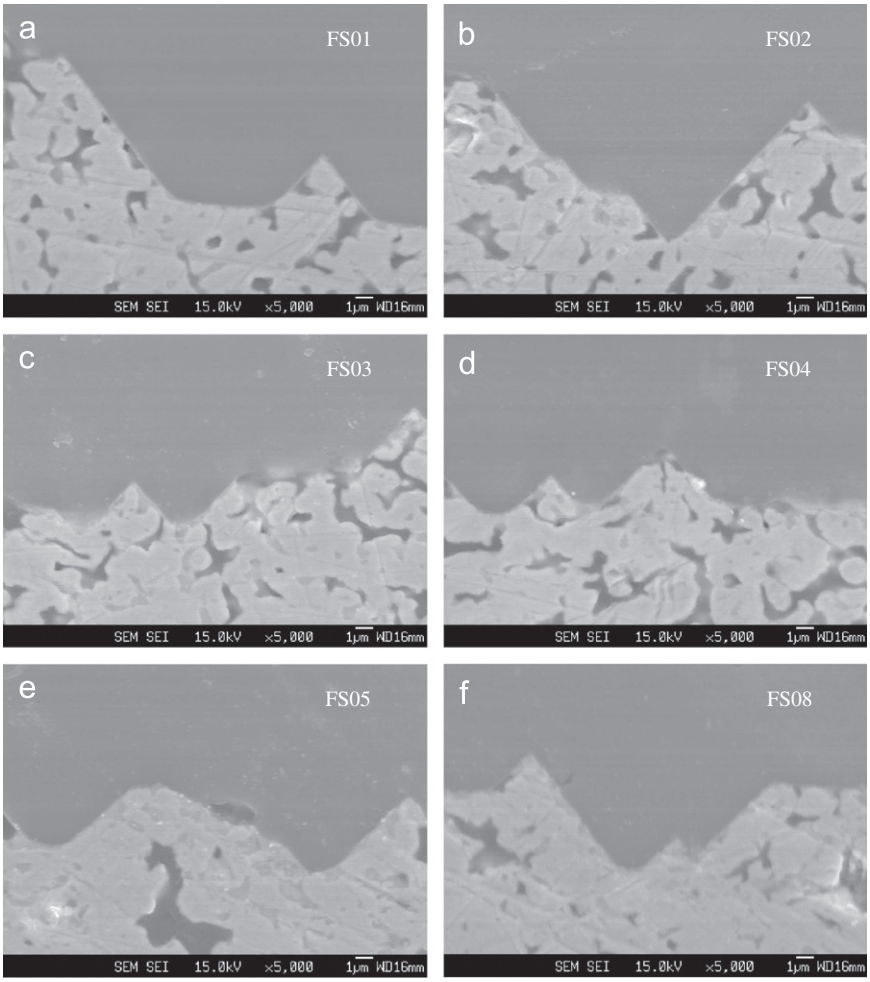

Fig. 7. Cross-sectional SEM images of the Ag–Si contact interface for (a) C1 (FS01), (b) C2 (FS02), (c) C3 (FS03), (d) C4 (FS04), (e) C5 (FS05) and (f) C8 cell (FS08 pastes).

layers as reported elsewhere [11]. In addition, Bi metals produced by reducing Bi_2O_3 can strongly influence the Ag–Si interface continuous contact structure since they could wet the metal surface providing a fluxing action which is caused by their low melting point (271.3 °C) as a function of Pb.

Current–voltage (*I–V*) curves of the C8 and C9 Si solar cells fabricated using lead-free silver paste (FS08) and leaded commercial silver paste (CN33-462) on emitters having a sheet resistance of 45 Ω/sq are shown in Fig. 8. In both type of cells, the reduction of the slope of the *I–V* curve can be observed at high voltage region. As noted in Table 2, there is also no great difference in the R_s between them. However, the *I–V* characteristic difference between C8 and reference C9 cell can be explained by the comparison of the R_{sh} value, conserving their flat *I–V* curve at the low voltage region. Obviously, the reference C9 cell degraded more rapidly than the lead-free C8 cell. There are several reasons for this cell performance difference. Leakage currents along the edges of cells and point defects in the p–n junction can lead to low R_{sh}. The point defects originate from impurities during the diffusion or metallization procedure into the n emitter [8]. Likewise, the effect of R_{sh} on *I–V* characteristics is well documented in the literature [7], where authors cited an influence of poor R_{sh} values as the key reason for the rapid degradation at the low voltage region. Similar to those indicated in Ref. [12], the poor R_{sh} value (4.3 Ω) for reference cell leads to rapid degradation curve in our results. Owing to the same in all experimental respects except for the metallization source in this study, this

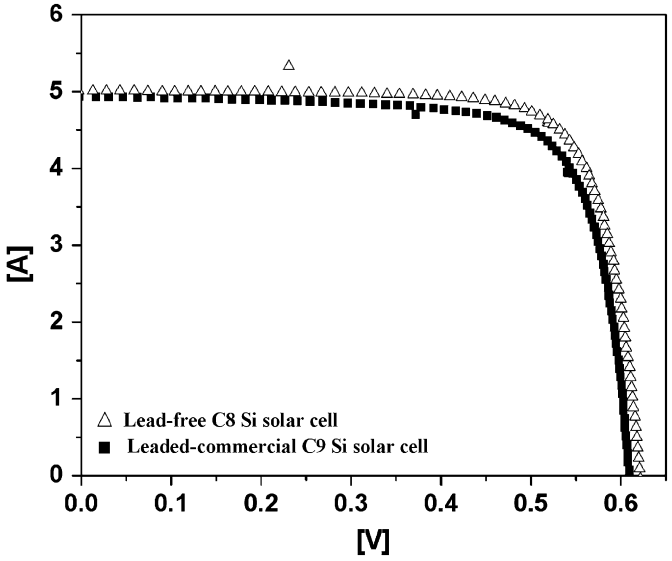

Fig. 8. Current–voltage (*I–V*) curves of the C8 and C9 Si solar cells fabricated with lead-free silver paste (FS08) and leaded commercial silver paste (CN33-462) on emitters having a sheet resistance of 45 Ω/sq.

degradation curve at the low voltage region may be due to the injection of impurities from the front Ag paste into the Ag/n-type Si interface regions during the firing step. Therefore, it seems

reasonable to conclude that the difference of the metallization source containing a glass frit has mainly caused a variation in R_{sh} values, which in turn has caused rapid degradation at the low voltage region.

In short, for the reference cells, the outcome of rapid degradation at the low voltage region is attributed to the poor R_{sh}, which has attracted lower FF. Thus, narrower area underneath the I–V characteristic is filled by the rectangle $V_m I_m$ relation to the rectangle $V_{oc} I_{sc}$. It is therefore clear that lower FF is due to the effect of R_{sh}.

4. Conclusion

The lead-free front contact silver pastes having the optimized values of R_s and R_{sh} at conventional firing temperature was formulated and the effects of the content and size of glass frits on the front metallization and electrical performance of the resulting cell were investigated. By virtue of the glass frit control and formulated inorganic additives, the solar cell of 156 μm area using Cz Si substrate was fabricated in a mass-production environment. The resulting cell achieved an efficiency close to 16.5% with a maximum FF of 77.3%. The optimum lead-free silver pastes formulation for better conductivity, higher density of the silver matrix compact and continuous contact metallization could be designed by the addition of the inorganic additives with the smallest glass frit of 3.05 wt% in pastes. R_{sh} and FF values of the optimized cell were slightly higher when compared with the commercial leaded Ag paste, although cells were fabricated by metallizing the lead-free silver pastes. Important results of this study can be summarized as follows:

(1) The pastes containing glass frits with a large mean particle size do not allow continuous contact formation in Si–Ag alloys due to the poor contact and metallization quality. The cells fabricated using these pastes tend to have a higher junction shunting and leakage rate.
(2) Higher R_{sh} and lower R_s values were attributed to the use of the glass frit with a small mean particle size and shallow silver penetration depth into Si from Ag–Si interface regions. Eventually, the high FF_s and conversion efficiencies could be obtained by using less amount of glass frit when the glass frit with a small mean particle size was used.
(3) Control techniques of glass frits can have an influence on silver front contact metallization quality during the firing step and what ultimately determines the contact quality is how well glass frits are controlled in precise amounts and its size.
(4) The cells containing a mixture of Bi_2O_3 as an inorganic binder and CaO or MgO as functional material with low junction barriers in metal/n-type Si interface regions show the lowest R_s values and also possess high FF_s. The cells containing Bi_2O_3 show relatively less voids and better metallization quality after being fired.

References

[1] European directive RoHS, 2002/95/EC.
[2] M. Bahr, S. Kim, S. Sridharan, C. Khadilkar, J. Lossen, S. Dauwe, On lead and cadmium free metallizations for industrial solar cells and modules, in: Proceedings of the 21st European Photovoltaic Solar Energy Conference, Dresden, Germany, 2006, pp. 859–864.
[3] J. Hoornstra, G. Schubert, K. Broek, F. Granek, C. LePrince, Lead free metallisation paste for crystalline silicon solar cells: from model to results, in: Proceedings of the 31st IEEE Photovotaic Specialists Conference, Florida, 2005, pp. 651–654.
[4] T. Lauinger, J. Moschner, A.G. Aberle, R. Hezel, Optimization and characterization of remote plasma-enhanced chemical vapor deposition silicon nitride for the passivation of p-type crystalline silicon surfaces, J. Vac. Sci. Technol. A 16 (1998) 530–543.
[5] M. Hilali, A. Rohatgi, S. Asher, Development of screen-printed silicon solar cells with high fill factors on 100 Ω/sq emitters, IEEE Trans. Electron. Dev. 51 (2004) 948–955.
[6] S.B. Rane, T. Seth, G.J. Phatak, D.P. Amalnerkar, Effect of inorganic binders on the properties of silver thick films, J. Mater. Sci. Mater. Electron. 15 (2004) 103–106.
[7] T. Markvart, L. Castaner, Solar Cells: Materials, Manufacture and Operation, Elsevier, New York, 2005, pp.6–15.
[8] A. Goetzberger, J. Knobloch, B. VoB, Crystalline Silicon Solar Cells, John Wiley and Sons, Chichester, 1998, pp. 69–79.
[9] S. Sridharan, C. Khadilkar, T. Pham, A. Shaikh, Characterization of silver/glass/silicon front contact interface in a silicon solar cell, in: 13th Workshop on Crystalline Silicon Solar Cell Materials and Processes, Vail, Colorado, 2003, pp. 162–165.
[10] C. Khadilkar, S. Kim, T. Pham, A. Shaikh, S. Sridharan, Characterization of silver front contact in a silicon solar cell, Technical Digest of the International PVSEC-14, Bangkok, Thailand, 2004, pp. 635–638.
[11] C. Ballif, D.M. Huljic, G. Willeke, A. Hessler-Wyser, Silver thick-film contacts on highly doped n-type silicon emitters: structural and electronic properties of the interface, Appl. Phys. Lett. 82 (2003) 1878–1880.
[12] I. Perez-Quintana, A. Marttel, L. Hernandez, Comparative study of metal–semiconductor contact degradation by current pulses on silicon solar cells with two contact types, Solid-State Electron. 45 (2001) 2017–2021.